International Journal of Nanomedicine

Dovepress

open access to scientific and medical research

Open Access Full Text Article

ORIGINAL RESEARCH

Small Extracellular Vesicles Released from Bioglass/Hydrogel Scaffold Promote Vascularized Bone Regeneration by Transferring miR-23a-3p

Hongxing Hu[1], Hang Zhang[2], Ziheng Bu[3], Zhongtang Liu[3], Fang Lv[4,5], Mingmang Pan[5], Xuan Huang[3], Liming Cheng[1]

[1]Department of Orthopedics Tongji Hospital Affiliated to Tongji University, Tongji University School of Medicine, Shanghai, People's Republic of China; [2]School of Mechanical Engineering, Shanghai Jiao Tong University, Shanghai, People's Republic of China; [3]Department of Orthopedics Changhai Hospital Affiliated to the Second Military Medical University, Shanghai, People's Republic of China; [4]Shanghai Key Laboratory of Regulatory Biology, Institute of Biomedical Science and School of Life Science, East China Normal University, Shanghai, People's Republic of China; [5]Department of orthopedics, Shanghai Fengxian District Central Hospital, Shanghai, People's Republic of China

Correspondence: Xuan Huang, Department of Orthopedics Changhai Hospital Affiliated to the Second Military Medical University, 168 Changhai Road, Shanghai, People's Republic of China, Tel +86 18930172772, Email 11791709@qq.com; Liming Cheng, Department of Orthopedics Tongji Hospital Affiliated to Tongji University, Tongji University School of Medicine, 389 Xincun Road, Shanghai, People's Republic of China, Tel +86-21-56051080, Email limingcheng@tongji.edu.cn

Background: The treatment of critical-size bone defect is a great difficulty in orthopedics. Osteogenesis and angiogenesis are critical issue during the process of bone repair and remodeling. Mesenchymal stem cells (MSCs)-derived exosomes have the same therapeutic effect to MSCs-based therapies. The effect of human umbilical cord MSCs-derived sEVs (hUC-MSCs-sEVs) on vascularized bone regeneration and the potential mechanism remains to be investigated. Herein, we aimed to explore the therapeutic effect and the mechanism of hUC-MSCs-sEVs on critical-size bone defect.

Methods: To investigate the potential osteogenesis and angiogenesis effects of sEVs in vitro, we extracted sEVs from hUC-MSCs, and then sEVs were co-incubated with BMSCs and HUVECs. We next investigated the effect and potential mechanism of sEVs on the effects of osteogenesis and angiogenesis. We fabricated 3D-printed bioglass scaffold with Gelma/nanoclay hydrogel coatings to load sEVs (BG-gel-sEVs) to ensure in vivo sustained efficacy of sEVs. Finally, the skull defect model was used to evaluate the capacity of vascularized bone regeneration of the composited scaffolds.

Results: hUC-MSCs-sEVs facilitated calcium deposition and the endothelial network formation, inducing osteogenic differentiation and angiogenesis by delivering miR-23a-3p to activate PTEN/AKT signaling pathway. Additionally, the BG-gel-sEVs composited scaffold achieved vascularized bone regeneration in vivo.

Conclusion: This finding illuminated that hUC-MSCs-sEVs promoted osteogenesis and angiogenesis by delivering miR-23a-3p to activate PTEN/AKT signaling pathway, achieving vascularized bone regeneration.

Keywords: small extracellular vesicles, bone regeneration, angiogenesis, miR-23a-3p, bioglass scaffolds

Introduction

The treatment of critical-size bone defect occurred by the bone diseases such as osteoporosis, bone infection, osteonecrosis, bone tumor and other diseases is a great difficulty in orthopedics.[1] Osteogenesis and angiogenesis are critical issue during the process of bone repair and remodeling. Angiogenesis is an essential process for high-quality bone regeneration due to its critical role in transportation of nutrients, growth factors, metabolic waste, and maintain the internal homeostasis of bone issue.[2] Currently, the treatments for bone defects include autologous grafts, allografts and bone tissue engineering.[3] Autologous grafts have some limitations including secondary injuries, limited quantity of bone and morbidity at the donor site.[4] While allografts may have the disadvantage of immunogenic rejection.[5] Nowadays, mesenchymal stem cells (MSCs)-based tissue engineering has been considered as an alternative strategy.[6,7] As one of the most abundant subsets of stromal cells, MSCs show positive

Received: 19 September 2022
Accepted: 23 November 2022
Published: 9 December 2022

surface marker of CD73, CD105 and CD105 with negative expression of CD14, CD11b, CD19, CD34, CD45, CD79a and HLA-DR.[8,9] MSCs show multidirectional differentiation potential in vitro.[8] However, the reliability of MSC-based therapy was affected by MSC heterogeneity including donor heterogeneity, tissue source heterogeneity and cell immunophenotype heterogeneity.[10–12] Therefore, novel promising strategies to repair critical-size bone defect are desperately needed.

Recent evidence indicated that MSCs-derived exosomes which was largely acquired via the paracrine mechanism have the same therapeutic effect to MSCs-based therapies.[13] Human umbilical cord MSCs (hUC-MSCs) show satisfied biological properties, such as rich sources, desirable proliferation capability and facilitated acquisition process.[14] Small extracellular vesicles (sEVs)-derived MSCs revealed specific advantages than MSCs, including high stability, facilitated acquisition and abundant source.[15,16] Previous study reported that human dental pulp stem cells derived small extracellular vesicles (MSCs-sEVs) promoted bone regeneration.[17] However, the effect of hUC-MSCs-derived sEVs (hUC-MSCs-sEVs) on vascularized bone regeneration and the potential mechanism remains to be investigated.

Exosomes are a kind of sEVs with a size of 30–150nm, containing various proteins, miRNA, ncRNA and growth factors.[18–20] MicroRNAs are a kind of small single-strand noncoding RNAs, which mediate target genes silencing by translational repression or mRNA degradation.[21,22] Previous studies indicated that sEVs delivered miRNA to mediate intercellular communication and regulate function of recipient cell,[23,24] indicating miRNAs were critical issue in sEVs-mediated cell-to-cell communication. Our group previously demonstrated that hUC-MSCs-sEVs contained abundant miR-23a-3p contributed to repair cartilage through promoting the formation of glycosaminoglycan, extracellular matrix synthesis and collagen deposition.[25] However, whether hUC-MSCs-sEVs could enhance angiogenesis and osteogenesis to repair critical-size bone defect by delivering miR-23a-3p remained further researched.

For cartilage,[26] skin[27,28] or bone[29] tissue engineering technology, sEVs have been always entrapped into hydrogel to achieve localization and slow-release to enhance vascularization or facilitate tissue regeneration. However, these hydrogels cannot protect some soft tissue like the brain before new bone regeneration due to their weak mechanical properties.[30] Additionally, hydrogel with high strength alone fail to bond to the subchondral layer or enhance bone regeneration since high water content and lack of osteo-conduction.[5,31] 3D-printed scaffolds with excellent physic-chemical composition and mechanical property are the ideal biomaterial in cell-free bone tissue engineering.[4,32] In our previous work, we fabricated Gelatin methacrylate (Gelma)/nanoclay hydrogel with the nice function of sustained release of sEVs.[25] Therefore, in this study, we fabricated 3D-printed bioglass (BG) scaffold with Gelma/nanoclay hydrogel coatings to load sEVs to achieve cell-free bone regeneration.

As shown in Scheme 1, in this work, we prepared the BG-gel-sEVs composited scaffold for the repair of calvarial bone defect. The therapeutic sEVs released from BG scaffold with Gelma/nanoclay hydrogel coatings were uptaken by BMSCs and endothelial cells. The internalized sEVs facilitated calcium deposition and the endothelial network formation, inducing osteogenic differentiation and angiogenesis by delivering miR-23a-3p. The ideal bone regeneration was achieved by the therapeutic BG-gel-sEVs composited scaffold and this finding may be a potential treatment for the repair of critical-size bone defect.

Materials and Methods

Cell Culture

hUC-MSCs (Cyagen, HUXUC-01001, China) were incubated in the medium (Lonza, 12–725F, USA) supplemented serum (Life Science, 259,509, USA). The multipotency of hUC-MSCs were verified by inducing hUC-MSCs to osteogenic, chondrogenic, adipogenic cells. The surface marker of MSCs was verified by flow cytometry analysis.

Isolation and Characterization of sEVs

According to the established protocol,[25] sEVs were isolated from the medium of hUC-MSCs. Briefly, hUC-MSCs were cultured in serum-free medium for 72 hours. The collected supernatants was centrifuged (300×g for 10 min, 2000×g for 10 min, and 10,000×g for 30 min at 4°C) to removed cell debris and dead cells. Then, the supernatants were transferred to the new ultracentrifuge tube and then centrifuged at 100,000×g for 70 min (4°C). The supernatants were centrifuged again to isolate sEVs.

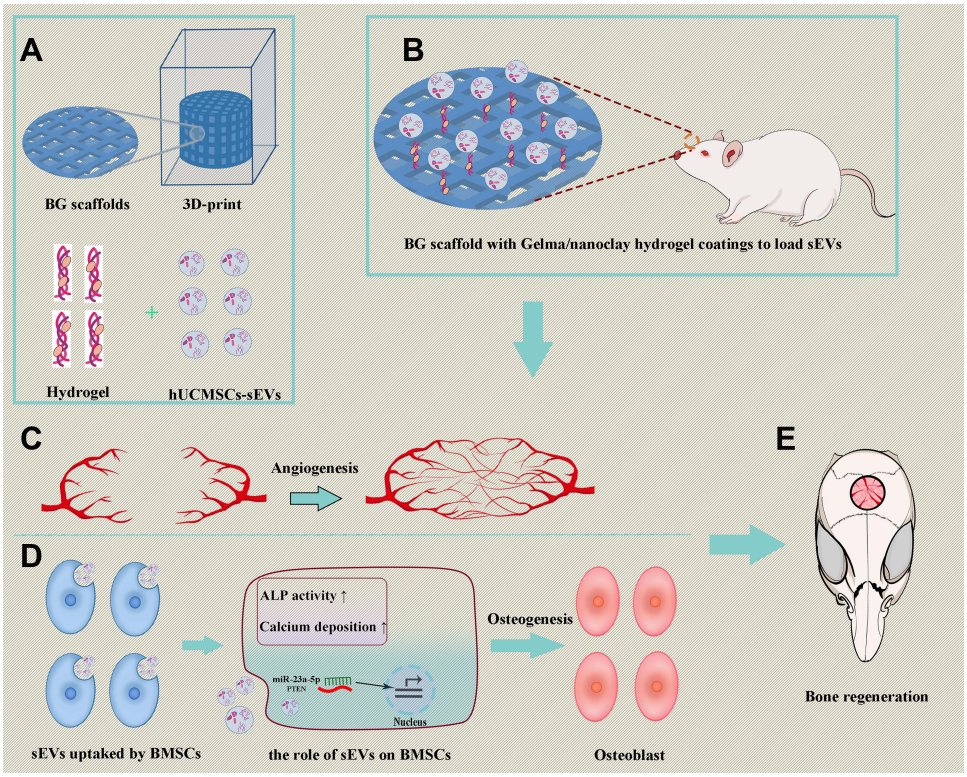

Scheme 1 Schematic illustration of small extracellular vesicles(sEVs) released by BG scaffold with Gelma/nanoclay hydrogel coatings (BG-gel-sEVs) for bone regeneration. (**A**) Fabrication of BG-gel-sEVs composited scaffolds. (**B**) Implantation of composited scaffold into critical-size calvarial bone defect. (**C** and **D**) The effect of therapeutic sEVs on angiogenesis and osteogenesis, respectively. (**E**) Regeneration of calvarial bone defect.

The size distribution and concentration of sEVs were analyzed by Nanosight NS300 system (Malvern, UK). The morphology of sEVs was identified by Transmission electron microscopy (TEM). The marker proteins of sEVs were identified through Western blotting.

PKH-26 Staining

According to the previous protocol,[25] sEVs were stained by PKH-26 staining kit (Sigma, MINI26, Germany). In brief, 100uL sEVs (10^8 particles/mL) were diluted by Dilution C solution and then the sEVs were stained by PKH-26 for 10 min in dark environment. The staining process was terminated by 1% bovine serum albumin. Then, the mixed solution was centrifuged at 100,000×g for 70 min (4°C). sEVs were obtained by resuspending the deposits with cold PBS. Bone marrow mesenchymal stem cells (BMSCs) were incubated with the labelled sEVs for 24h. Subsequently, 4% paraformaldehyde (PFA) was used to fix cells, and then the cells were marked with DAPI for 5 min. Fluorescence microscopy was used to visualize the stained cells.

Cell Proliferation Assay

According to the previous protocol,[33] BMSCs were isolated from the femur of 4–6 weeks old female C57BL/6 mice. To investigate cell viability, BMSCs were cultured in the α-MEM (contained 10% fetal bovine serum (Gibco, USA) and 1% penicillin and streptomycin) supplied sEVs for 24h and 48h. At the point time, according to the manufacturer's instructions, the cells were incubated with cell counting kit-8 (CCK-8, Dojindo, Kumamoto, Japan) for 3 h. OD values of 450nm were used to evaluate the cell activity.

ALP Activity Assay

As described previously,[34] BMSCs were cultured in the osteogenic differentiation medium (α-MEM with ascorbic acid, 1 μM dexamethasone, glycerol-2-phosphate, 10% fetal bovine serum, and 1% penicillin and streptomycin) contained

sEVs. At the point time (7 days), PFA was used to fix cells for 10 min. Subsequently, the fixed BMSCs were washed by PBS for three times. Then, the cells were cultured with 0.1% Triton X-100 for 10 min. Furthermore, after incubated with phosphate buffered saline with Tween-20 (PBST) for 10 min, the cells were stained with an ALP kit (Sigma, Germany) at 37°C for 30 min.

Calcium Deposition Assay

BMSCs were seeded in the osteogenic differentiation medium contained sEVs at a density of 1×10^4 cells/mL in a 24-well plate for 14 days. At the indicated time, PFA was used to fix cells for 10 min. Subsequently, ddH_2O were used to rinse cells, and then BMSCs were stained with alizarin red stain (ARS, Sigma, Germany) for 10 min.

Wound Healing Assay

The effect of sEVs on human umbilical vein endothelial cells (HUVECs) migration was assessed by "wound healing" assay in vitro. In brief, a sterile pipette was used to create "wound" after HUVECs growing in full density in 12 well plates. Then, PBS was used to rinse the cells to remove cell debris. HUVECs were cultured in the fresh medium containing sEVs for 8 h. Subsequently, the medium was removed and then fixed by PFA for 15min. The cells were stained with 0.2% crystal violet hydrate solution and then observed using microscope.

Tube Formation Assay

Matrigel™ matrix (Corning, 356,234, USA) was used to conduct angiogenesis assay in vitro. According to the previous protocol,[35] the plates and sterile pipettes were precooled at 4°C. 100uL Matrigel was added into cold 48-well plates using cold pipettes and then transferred to 37°C for solidification. Subsequently, HUVECs cultured on the complete medium contained sEVs were seeded on the solidified Matrigel. After incubation for 8 h, HUVECs were observed under inverted optical microscope. The number of nodes, junctions and branches were calculated by image J software.

Transwell Migration Assay

According to the established protocol,[36] transwell migration assay was implemented to evaluate the effect of sEVs on migration of BMSCs. In brief, BMSCs incubated in the medium without serum were seeded the upper chamber of transwell system (BD falcon, USA). After 8 h migration, BMSCs were fixed by 4% PFA. Then, 0.2% crystal violet was used to stain the migrated cells, and the cells on the upper chamber were removed. The microscopy was used to visualize the migrated BMSCs.

Real-Time Quantitative Polymerase Chain Reaction (qPCR) Assay

Osteogenic differentiation medium supplemented sEVs were implemented for BMSCs incubation. After incubating for 14 days, TRIzol reagent (Invitrogen Pty Ltd., Australia) was used to extract RNA. RevertAid First Strand cDNA Synthesis Kit (Thermo, USA) was used to achieve RNA reverse-transcribing. The mixture including the cDNA, SYBR, and the primers (OCN, BMP-2, and ALP) was added into the Optical 8-Cap strip, and then qPCR was performed. The primer sequence of above gene is listed in Supplementary Table 1.

Western Blot Assay

Western blot was carried out according to the previous protocol.[13] RIPA was used to harvest the cells, isolating endogenous proteins. BCA protein assay kit (Thermo, USA) was used to detect the concentration of the protein. Subsequently, equal amounts of proteins were separated by SDS-PAGE gel and then transferred to 0.22 μm polyvinylidene difluoride membranes. After being blocking by 5% fat-free milk, the membranes were incubated with primary antibodies overnight at 4°C. The membranes were rinsed by Tris buffered saline with Tween-20 (TBST) and then incubated with secondary antibodies for 1h at room temperature. ImmunoStar Western C (LI-COR, USA) was used to observe the protein band. The following primary antibodies were used. Anti-Akt (CST, USA, 9272, 1:1000), anti-phospho-Akt (CST, USA,9271, 1:1000), anti-PTEN (Promab Biotechnologies, China, 20,399, 1:1000), anti-GAPDH

(CST, USA, 2118, 1:1000), anti-β-actin (CST, USA,3700, 1:1000), anti-CD63 (SBI, USA, EXOAB-CD63A-1, 1:1000), anti-CD81 (SBI, USA, EXOAB-CD81A-1, 1:1000), CD9 (SBI, USA, EXOAB-CD9A-1, 1:1000).

Luciferase Reporter Assay and Transfection

Lipofectamine 2000 reagent (Invitrogen, 11,668,019, USA) was used to conduct luciferase reporter assay. According to the manufacturer's instruction, miR-23a-3p mimics and the luciferase report vectors were transfected into HEK-293t cells. Passive lysis buffer was used to cleave the cells after 24 hours transfection. Dual-Luciferase Reporter Assay System (Promega, USA) was used to calculated firefly and renilla luciferase activity.

Antagomir-23a-3p Treatment

According to the previous described,[25] the cells were cultured with antagomir-23a-3p or scramblemir (Ctrl) in serum-free medium for 6h. Subsequently, the supernatant was removed and then the cells were incubated in the completed medium. The sequences of antagomir-23a-3p and scramblemir are shown in Supplementary Table 2.

Construction and Characterization of 3D BG-Gel Scaffold

Construction of Osteogenic 3D BG/Gel Scaffold

Bioglass scaffolds were fabricated by digital light processing (DLP) printing technique and sintering process.[37] Gelma/nanoclay hydrogel was fabricated as previously described.[25] The scaffold was soaked in 100uL Gelma/nanoclay hydrogel solution containing 10uL sEVs (10×10^{10} particles/mL) and then radiated by 365 nm UV for 2 min to coat sEVs film.

The sEVs released profiles from the scaffolds were calculated by BCA (Thermo, USA) according to the established protocol.[28] In brief, the scaffolds added into the upper chamber were soaked in 100 uL PBS which was added into the lower chamber of Transwell insert (Corning, USA). At the point time, the cultured PBS was collected and replaced by 100uL fresh PBS. Then, BCA was used to quantify the profiles of the released sEVs.

Scanning Electron Microscopy (SEM)

SEM was implemented to observe the structure of the scaffolds and the distribution of sEVs on the scaffolds. The scaffolds coated with sEVs were freeze-dried. After sputter-coated with gold for 30s, the samples were visualized by SEM.

Live and Dead Assay

As previously described,[38] to evaluate the viability of the scaffolds immobilized sEVs, BMSCs were seeded in the scaffold at a density of 1×10^4 cells/mL in a 24-well plate for 24 h. Then, the cells on the scaffolds were stained by Live/Dead staining kit (Invitrogen, USA). The fluorescent images were obtained by fluorescence microscopy.

Biocompatibility and Cytotoxicity Assay

The cytotoxicity of the scaffolds was evaluated using CCK-8 assay. Briefly, 1×10^4 cells/mL BMSCs were seeded on the samples and incubated for 1, 3, and 7 days. The viability of BMSCs examined by CCK-8 reflected the cytotoxicity of the scaffold. Data were presented as mean ± SD of three number of replicates.

Animal Experiments

All surgical procedures required the agreement of the ethical review committee of Tongji Hospital affiliated Tongji University and conducted in strict conformity with China's Guidelines for the Ethical Review of Laboratory Animal Welfare. Eighteen male BALB/C mice (8 weeks old) were anaesthetized by injecting avertin. A sagittal incision of 1.5–2.0 cm was made on the scalp and then 5 mm diameter critical-size defect was made on center of cranium by an electric trephine drill (STRONG204). To avoid damage to the dura and brain, the operation procedure was very careful. Then, the scaffolds contained sEVs were implanted into the defect. Moreover, calcein AM (green), alizarin red (red) were injected intramuscularly into these skull defect model mice at 5 and 9 weeks, respectively. Additionally, to evaluate the regenerated blood vessel in bone defect region after 12 weeks, mice were perfused with Microfill (MV-122, Flow Tech) after euthanasia, and then the skulls were decalcified and then for micro-CT analysis.

Microcomputed Tomography (Micro-CT)

The animals were sacrificed at the pointed time (12 weeks post-surgery) and the targeted skulls were collected. The samples were fixed by 4% paraformaldehyde for 48h and rinsed by dd H_2O. Micro-CT (SkyScan1176, Bruker) was used to evaluate the regeneration of the new bone and blood vessels. The bone and blood vessels were 3D reconstructed by CTvox and then analyzed by CT analysis to obtain the bone tissue volume/total tissue volume (BV/TV), trabecular separation/spacing (Tb.Sp), bone mineral density (BMD) and trabecular thickness (Tb.Th).

Histology and Immunohistochemical Analysis

The samples were decalcified in EDTA and then dehydrated in a gradient alcohol. After being embedded in paraffin, the skulls were cut into 6 μm thickness. Hematoxylin/eosin (HE), Masson trichrome and van gieson (VG) staining were performed to estimate the regeneration of the new bone. The regeneration of bone was quantificationally analyzed by ImageJ software. The sequential fluorescent labeling of non-decalcified skull samples was observed under the fluorescent microscope. Immunohistochemical staining was carried out as previously described.[39]

Statistical Analysis

Quantitative data were presented as the mean ± standard deviation (SD). Comparation between two groups was performed by the unpaired Student's *t*-test. For the analysis of multiple groups, one-way analysis of variance (ANOVA) was used. Statistical analysis was carried out by Graph pad prism 7. $P < 0.05$ was considered to be statistically significant.

Results

Identification and Characterization of hUC-MSCs and hUC-MSCs-sEVs

When hUC-MSCs were cultured to reach 80% confluence, the cells showed spindle-like shape under the microscope (Figure 1A). To further follow the criteria of stem cell, flow cytometric was used to analyze the surface marker of cells. As illustrated in Figure 1B, hUC-MSCs were positive for CD73, CD166, CD105, CD44 and negative for CD45 and CD34. Moreover, hUC-MSCs could be induced to adipogenic, osteogenic and chondrogenic cells (Supplementary Figure 1). As illustrated in Figure 1C, sEVs showed a spherical microvesicle morphology with double membrane structure. Based on measure of nanoparticle tracking analysis, the average diameters of the hUC-MSCs-sEVs were about 155.9 nm (Figure 1D). Moreover, Western blot analysis demonstrated that the extracellular vesicles-related specific marker including CD63, CD81, CD9 were highly expressed on sEVs, whereas actin was absent on sEVs (Figure 1E). Taken together, the above results indicated that hUC-MSCs-sEVs were successfully isolated from the supernatants of hUC-MSCs.

hUC-MSCs-sEVs Enhanced the Proliferation, Migration and Osteogenic Differentiation of BMSCs

We used PKH-26 staining kit to label hUC-MSCs-sEVs. Then, sEVs were co-cultured with BMSCs for 24h. As illustrated in Figure 2A, sEVs stained in red fluorescence were up-taken by BMSCs whose nuclei was stained in blue fluorescence by DAPI. Subsequently, we used CCK-8 assay to measure the viability of BMSCs cultured with different concentration of hUC-MSCs-sEVs (Figure 2B), BMSCs were co-cultured with different concentration of sEVs (sEVs1 and sEVs2 meant that 5×10^8 and 10×10^8 particles/mL sEVs respectively). CCK-8 results showed that the number of BMSCs was significantly increased after sEVs treatment, and sEVs of 10×10^8 particles/mL significantly enhanced cell proliferation compared to sEVs of 5×10^8 particles/mL. Moreover, the transwell migration assay revealed that compared to the control group, the migrated ability of BMSCs on sEVs2 group was significantly increased. The number of migrated BMSCs co-incubated with sEVs of 10×10^8 particles/mL was significant than the sEVs1 group (Figure 2C and D). In addition, we used the ALP activity and calcium deposition assay to explore the osteogenic effect of hUC-MSCs-sEVs on BMSCs. Compared to the control and sEVs1 group, the sEVs2 group showed higher ALP positive area, as well as the calcium deposition assay evaluated by ARS staining (Figure 2E). Consistently, the osteogenic-related genes including

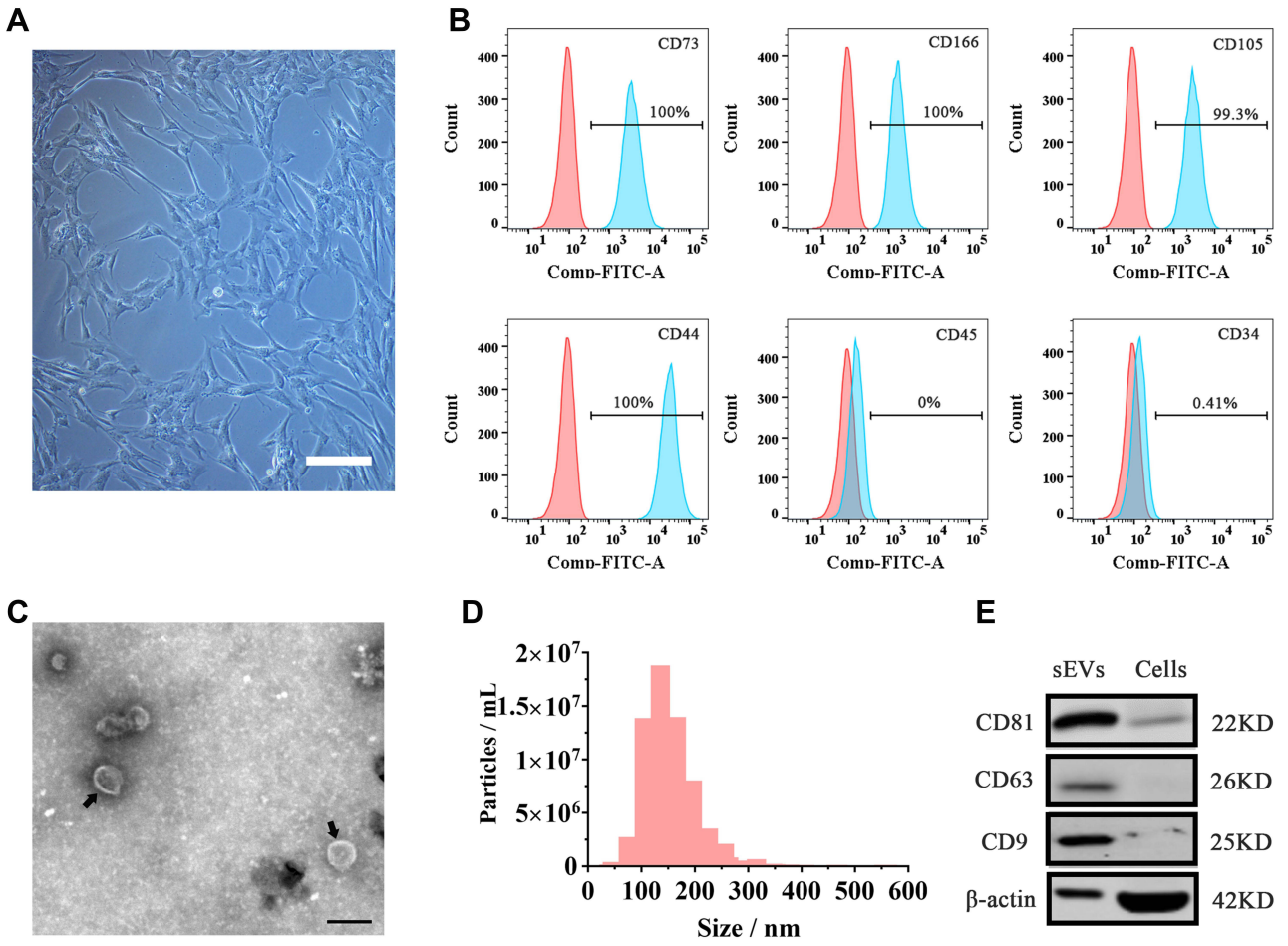

Figure 1 Characterization of hUC-MSCs and hUC-MSCs-sEVs. (**A**) hUC-MSCs exhibited spindle-like morphology. Scale bar: 100um. (**B**) Flow cytometric analysis of surface marker of hUC-MSCs. The red filled curves mean isotype control and the blue filled curves represent the surface marker of cells. (**C**) The morphology of hUC-MSCs-sEVs observed under transmission electron microscopy (TEM). Scale bar: 200nm. (**D**) Nanoparticle tracking analysis show the particle size of hUC-MSCs-sEVs. (**E**) The positive surface markers of hUC-MSCs-sEVs including CD9, CD63 and CD81 were determined by Western blot.

ALP, bone morphogenetic protein-2 (BMP-2), osteocalcin (OCN) were significantly increased after sEVs treatment. The sEVs2 group showed higher upregulation of the osteogenic-related genes compared to other groups (Figure 2F–H).

Angiogenic Effect of hUC-MSCs-sEVs in vitro

We then evaluated the angiogenic effect of hUC-MSCs-sEVs by stimulating the migration and endothelial network formation of HUVECs (Figure 3). PKH-26 staining kit was used to label hUC-MSCs-sEVs. The labelled sEVs in red fluorescence were endocytosed by HUVECs and mainly distributed in the cytoplasm (Figure 3A). Subsequently, we used CCK8 to estimate the effect of hUC-MSCs-sEVs on cell viability. HUVECs were co-incubated with sEVs for 24h, and the results showed that the number of cells treated with sEVs of 10×10^8 particles/mL was distinctly increased compared to sEVs of 5×10^8 particles/mL and control group (Figure 3B). Moreover, to evaluate the effect of hUC-MSCs-sEVs on migration ability of HUVECs (Figure 3C), we stimulated HUVECs with different concentration of sEVs (sEVs1 and sEVs2 meant that 5×10^8 and 10×10^8 particles/mL sEVs respectively) for 8h. Quantitative analysis indicated that the migration rate of sEVs2 group was significantly higher than other two groups (Figure 3D). Furthermore, matrigel-based assay was used to assess the effect of hUC-MSCs-sEVs on the endothelial network formation ability of HUVECs. As shown in Figure 3E, the endothelial network formation ability of HUVECs was improved after sEVs treatment, compared to the control group. Quantitative analysis including Nb nodes (Figure 3F),

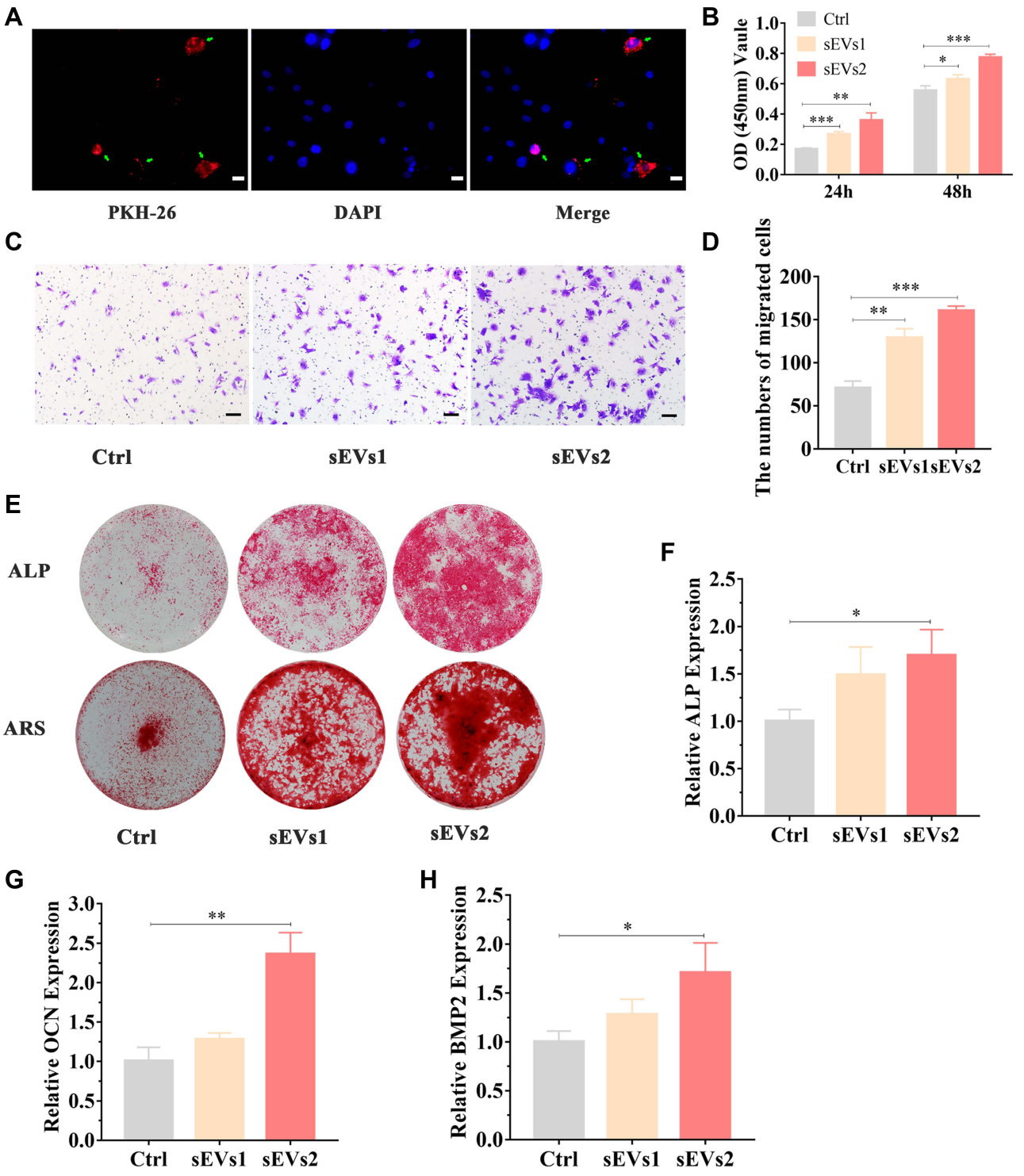

Figure 2 hUC-MSCs-sEVs enhanced the proliferation, migration and osteogenic differentiation of BMSCs. (**A**) Fluorescent micrograph of sEVs labeled by PKH-26. BMSCs were cultured with the labelled sEVs for 24 h. Scale bar:20um. (**B**) CCK-8 assay of BMSCs cultured with sEVs. *P < 0.05, **P < 0.01, ***P < 0.001. (**C**) Transwell assay of BMSCs cultured with sEVs for 8h. Scale bar: 50um. (**D**) Quantitative analysis of the number of migrated BMSCs. **P < 0.01, ***P < 0.001. (**E**) Alkaline phosphatase (ALP) activity and Alizarin Red S (ARS) staining of BMSCs. (**F–H**) The osteogenic-related gene of BMSCs cultured with different concentration of sEVs was measured via the qPCR, including osteocalcin (OCN), bone morphogenetic protein-2 (BMP-2), and ALP. *P < 0.05, **P < 0.01.

Nb junctions (Figure 3G) and Nb branches (Figure 3H) revealed that the number of nodes, junctions and branches was highest in sEVs2 group compared to other groups, indicating that 10×10^8 particles/mL significantly promoted the endothelial network formation ability of HUVECs.

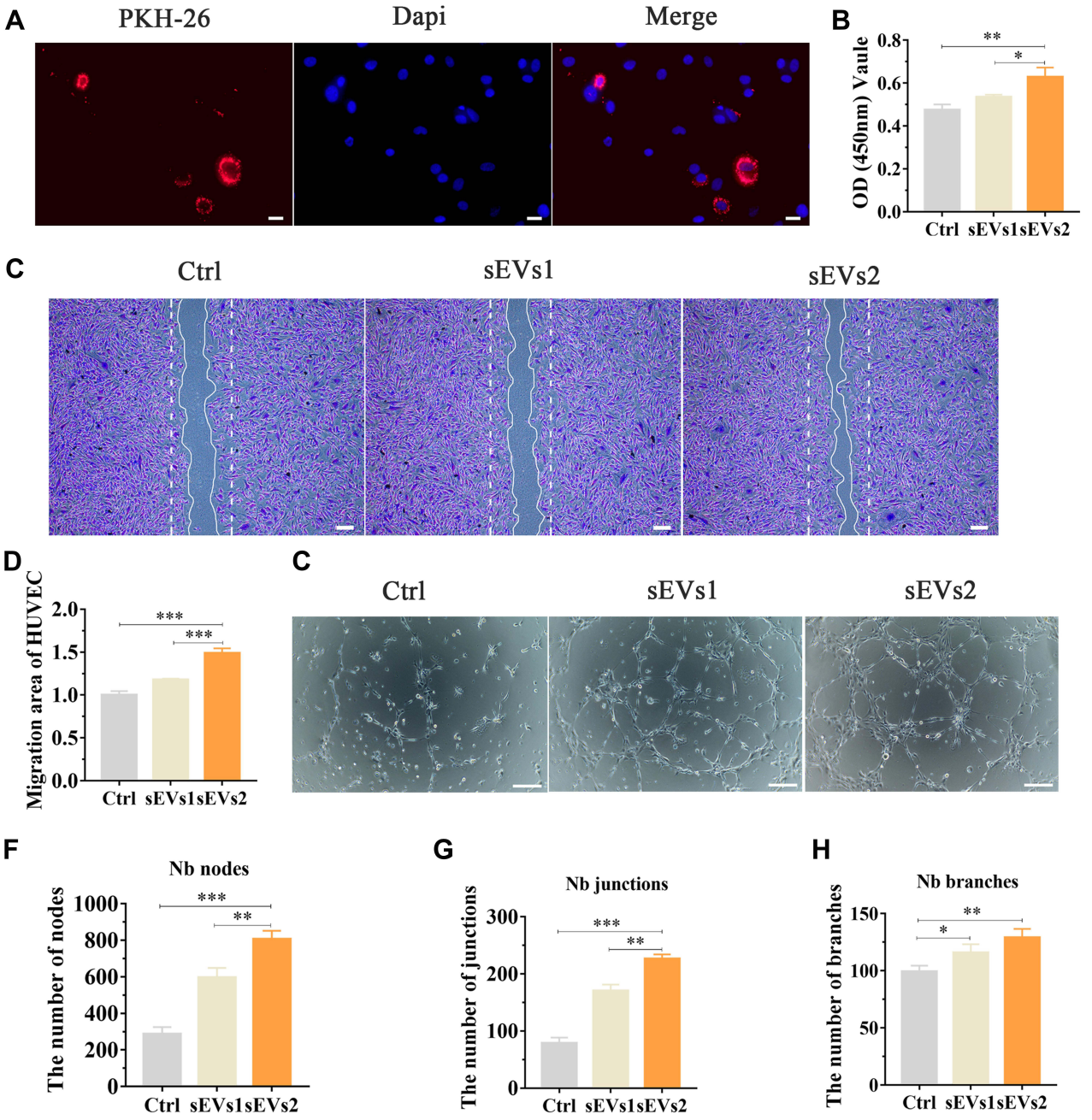

Figure 3 Angiogenic effect of hUC-MSCs-sEVs in vitro. (**A**) Fluorescent micrograph of sEVs labeled by PKH-26. HUVECs were cultured with the labelled sEVs for 24 h. Scale bar:20um. (**B**) CCK-8 assay of HUVECs cultured with sEVs for 24 h. *P < 0.05, **P < 0.01. (**C**) Representative images of "wound healing" assay of HUVECs after 8 h co-culture with hUC-MSCs-sEVs and (**D**) Quantitative analysis of the relative migrated percentage of HUVECs in different groups. ***P < 0.001. (**E**) Matrigel-based assay for HUVECs cultured with hUC-MSCs-sEVs. Scale bar: 100um. (**F**) Nb nodes, (**G**) Nb junctions, (**H**) Nb branches were all analyzed about tube formation assay by Image J. *P < 0.05, **P < 0.01, ***P < 0.001.

Exosomal miR-23a-3p Regulated the Expression of PTEN and AKT by Targeted 3'UTR of PTEN

sEVs have been demonstrated to transfer various miRNA to recipient cell to mediate intercellular communication.[40] Previous study showed miR-23a-3p was highly expressed in hUC-MSCs-sEVs and demonstrated that sEVs repair cartilage through transferring miR-23a-3p.[25] We next investigated the mechanism of exosomal miR-23a-3p in regulating osteogenesis and angiogenesis promoted by hUC-MSCs-sEVs (Figure 4). Subsequently, microRNA-target-predicting programs were used to predict the potential target genes of exosomal miR-23a-3p (Figure 4A). Among the predicted genes, PTEN has been

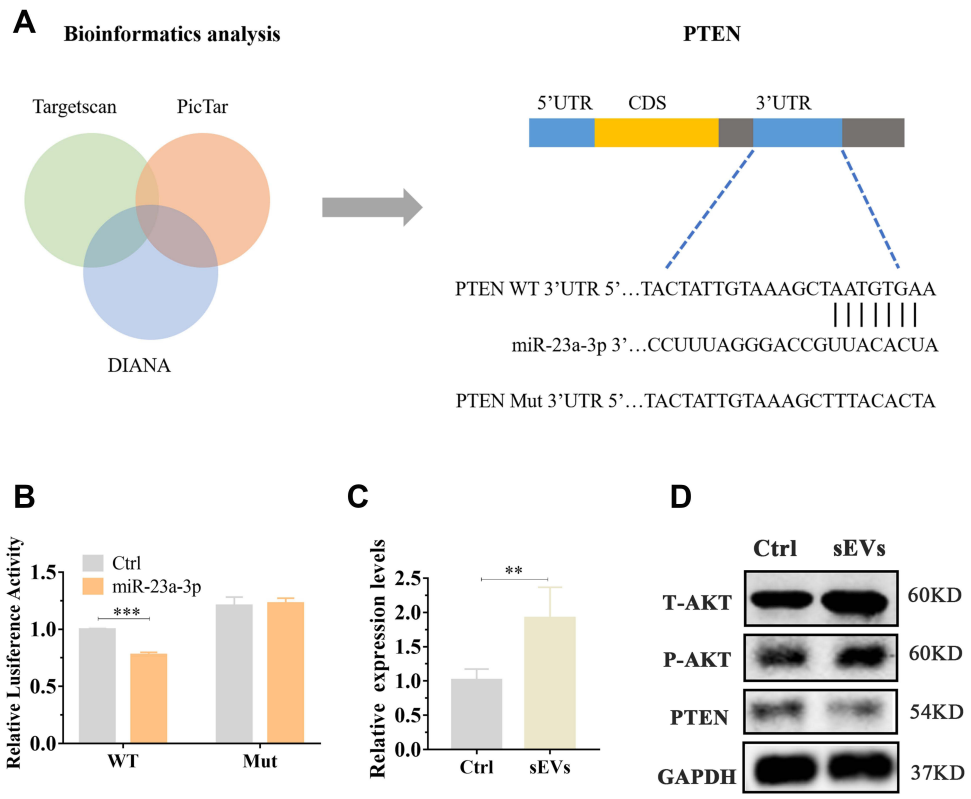

Figure 4 Exosomal miR-23a-3p regulated the expression of PTEN and AKT by targeted 3'UTR of PTEN. (**A**) The potential target sequence of miR-23a-3p was predicted by microRNA-target-predicting programs. (**B**) Luciferase reporter assay was carried out to demonstrate that PTEN is the target gene of miR-23a-3p. ***P < 0.001. (**C**) BMSCs were cultured with sEVs for 24h, then qPCR was used to measure miR-23a-3p expression level in BMSCs. Three independent replicates have been statistical analysis. **p < 0.01. (**D**) Western blot was implemented to evaluate the expression levels of AKT, P-AKT, PTEN in BMSCs.

demonstrated to play stimulatory role of osteogenic differentiation of BMSCs.[41] To demonstrate PTEN was a putative target of miR-23a-3p, luciferase reporter gene assay was performed. The constructs including WT-psicheck-PTEN and Mut-psicheck-PTEN were transfected into 293 T cells. The decline effect of luciferase activity induced by miR-23a-3p was abolished by mutating the binding site of 3'UTR of PTEN (Figure 4B). As shown in Supplementary Figure 2, the results of pull-down assay showed that PTEN RNA could be pulled down by bio-miR-23a-3p-WT, whereas bio-miR-23a-3p-Mut had no effect on PTEN expression. To further investigate whether hUC-MSCs-sEVs promoted osteogenesis and angiogenesis by delivering miR-23a-3p and activating downstream signaling pathways, BMSCs and HUVECs were cultured with sEVs. qPCR results revealed that miR-23a-3p expression was significantly increased in cells co-incubated with sEVs than the cells cultured in absence sEVs (Figure 4C and Supplementary Figure 3). Moreover, Western blot results showed that the expression level of T-AKT and P-AKT in cells co-incubated with sEVs were increased, whereas the expression level of PTEN was decreased (Figure 4D). Taken together, the above results proved that hUC-MSCs-sEVs promoted osteogenesis and angiogenesis in vitro by delivering miR-23a-3p, and the increased miR-23a-3p suppress the expression of PTEN, and then the inhibitory PTEN activated AKT signaling pathway.

miR-23a-3p Silencing Inhibited hUC-MSCs-sEVs-Mediated Osteogenesis and Pro-Angiogenesis in vitro

To examine the role of miR-23a-3p in hUC-MSCs-sEVs-mediated osteogenesis and angiogenesis in vitro, antagomirs-23a-3p was used to silence miR-23a-3p expression. We treated BMSCs and HUVECs with antagomirs-23a and then extracted RNA for qPCR analysis. The results showed that miR-23a-3p expression level was significantly decreased in ant-mir-23a groups when compared to control group (Figures 5A and 6A). Subsequently, we evaluated the effect of antagomirs-23a in hUC-MSCs

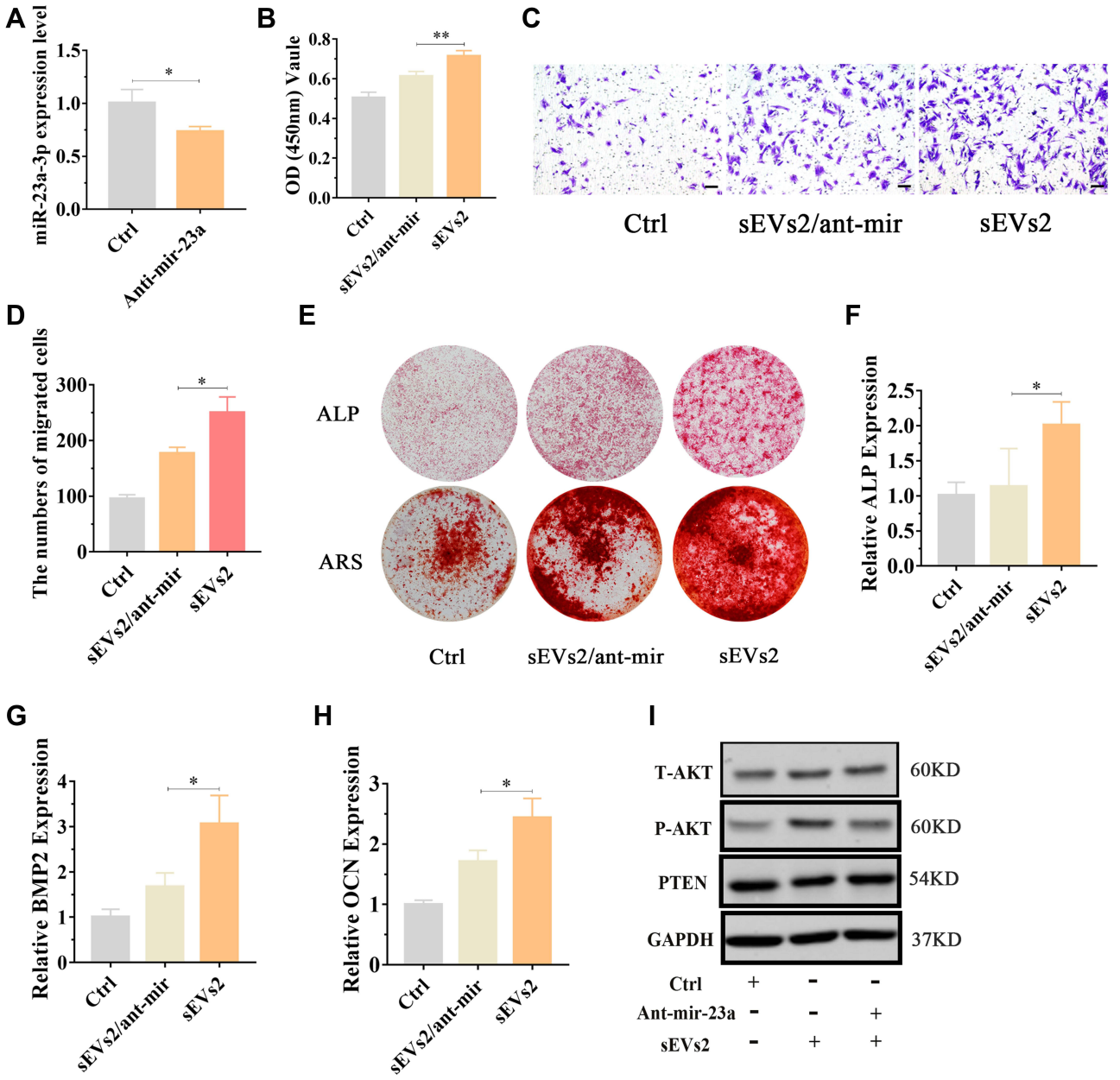

Figure 5 miR-23a-3p silencing alleviated hUC-MSCs-sEVs-mediated proliferation, migration and osteogenic differentiation of BMSCs in vitro by inhibiting PTEN/AKT signaling pathway. (**A**) BMSCs treated with sEVs were stimulated by antagomir-23a-3p or scramblemir (Ctrl) for 6 h, then qPCR was used to measured miR-23a-3p expression level. Three independent replicates have been statistical analysis. *P < 0.05. (**B**) Decreased cell proliferation in BMSCs after administration by antagomir-23a-3p and sEVs. Group sEVs2/ant-mir meant the applied of antagomir-23a-3p and hUC-MSCs-sEVs and group Ctrl meant scramblemir. Three independent replicates have been statistical analysis. **P < 0.01. (**C**) Transwell assay of BMSCs which were cultured with scramblemir (Ctrl), sEVs2/ant-mir and sEVs2. (**D**) Quantitative analysis of transwell assay. Three independent replicates have been statistical analysis. *P < 0.05. (**E**) Alkaline phosphatase (ALP) activity and Alizarin Red S (ARS) staining of BMSCs which were cultured with scramblemir (Ctrl), sEVs2/ant-mir and sEVs2. (**F–H**) Measurement of expression levels of the osteogenic-related gene of BMSCs cultured with scramblemir (Ctrl), sEVs2/ant-mir and sEVs2 via the qPCR, including, ALP, BMP-2 and OCN. *P < 0.05. (**I**) Western blotting assay of PTEN/AKT signaling pathway protein including T-AKT, P-AKT and PTEN.

-sEVs-mediated osteogenesis and angiogenesis in vitro. As shown in Figures 5B and 6B, antagomir-23a-3p remarkably reduced the cell proliferation induced by hUC-MSCs-sEVs. The number of migrated BMSCs was significantly decreased after antagomirs-23a-3p treatment, indicating that the favorable migration effect induced by sEVs was impaired by antagomirs-23a-3p (Figure 5C and D). In addition, the ALP activity and calcium deposition assay evaluated by ARS staining showed that antagomirs-23a-3p reduced the ALP activity induced by hUC-MSCs-sEVs, as well as the calcium deposition assay (Figure 5E). Moreover, antagomirs-23a-3p remarkably decreased the expression of osteogenic-related genes including

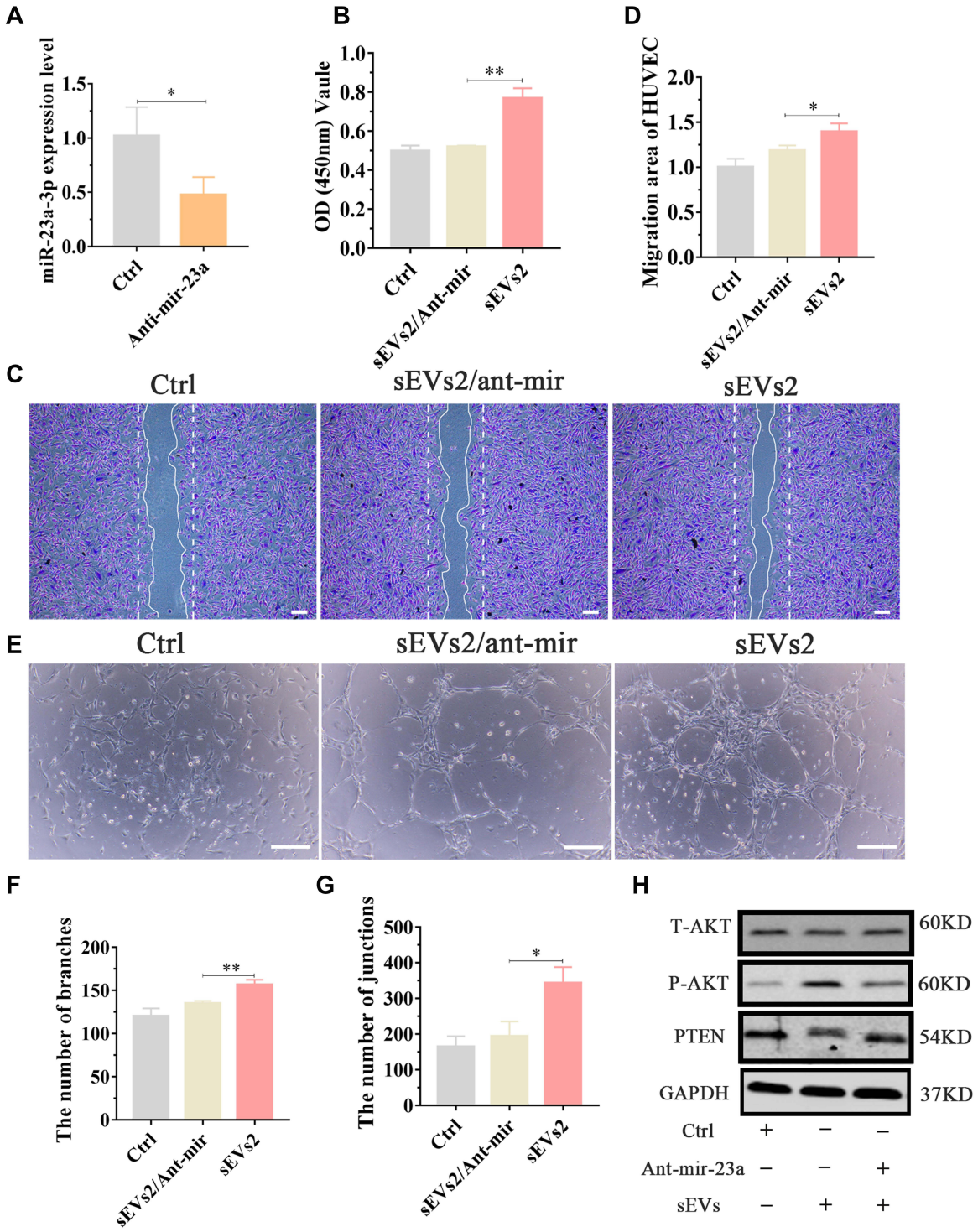

Figure 6 miR-23a-3p silencing alleviated hUC-MSCs-sEVs-mediated pro-angiogenic effect in vitro. (**A**) HUVECs treated with sEVs were cultured with antagomir-23a-3p or scramblemir (Ctrl) for 6 h, and then qPCR was used to measured miR-23a-3p expression level. *P < 0.05. (**B**) CCK-8 assay of BMSCs cultured with scramblemir (Ctrl), antagomir-23a-3p and hUC-MSCs-sEVs. **P < 0.01. Three independent replicates have been statistical analysis. (**C**) Representative images of "wound healing" assay of HUVECs after 8 h co-culture with scramblemir (Ctrl), antagomir-23a-3p and hUC-MSCs-sEVs, and (**D**) Quantitative analysis of the relative migrated percentage of HUVECs in different groups. Three independent replicates have been statistical analysis. *P < 0.05. (**E**) Matrigel-based tube formation assay for HUVECs cultured with scramblemir (Ctrl), antagomir-23a-3p and hUC-MSCs-sEVs. Scale bar: 100um. (**F**) Nb branches and (**G**) Nb junctions, were all analyzed about tube formation assay by Image J. Data was presented as mean ± SD of three number of replicates. *P < 0.05, **P < 0.01. (**H**) Western blotting assay of PTEN/AKT signaling pathway protein including T-AKT, P-AKT and PTEN. Group Ctrl and sEVs2 meant scramblemir and 10×10^8 particles/mL hUC-MSCs-sEVs, respectively.

ALP, OCN and BMP-2 mediated by hUC-MSCs-sEVs (Figure 5F–H). Additionally, antagomirs-23a-3p significantly reduced the favorable migration of HUVECs which was induced by sEVs (Figure 6C and D). Similarly, endothelial network formation ability of HUVECs induced by sEVs was obviously reduced by antagomirs-23a-3p (Figure 6E–G). Furthermore, the results of Western blot showed that when treated antagomir-23a-3p, T-AKT, P-AKT expression level of in cells were decreased, whereas PTEN expression level was increased (Figure 5I and Figure 6H), demonstrating that antagomir-23a-3p impaired sEVs-mediated activation of AKT signaling pathway. Collectively, above results demonstrated that miR-23a-3p silencing attenuated the osteogenic and pro-angiogenic effect induced by hUC-MSCs-sEVs in vitro.

Characterization and Release Kinetics of Engineered BG Composited Scaffolds

SEM confirmed the changes of the surface morphology of the scaffolds (Figure 7A). Live/dead staining assay was performed to investigate the cytotoxic effect of samples. As showed on (Figure 7B), the live BMSCs stained with green fluorescence adhere and survive well on the surface of these scaffolds, and there were few dead cells in red fluorescence, indicating that the scaffolds exhibited favorable cytocompatibility and were suitable for cell growth. To further investigate the sEVs release kinetics in BG-sEVs and BG-gel-sEVs scaffolds, the scaffolds were soaked in PBS for 1,3,7 days. At the pointed time, the scaffolds were visualized under the fluorescence microscope. As seen from (Figure 7C), more red dots which meant PKH-26 labeled sEVs were observed on the BG-gel-sEVs scaffolds, compared to that on the BG-sEVs scaffold, indicating that sEVs

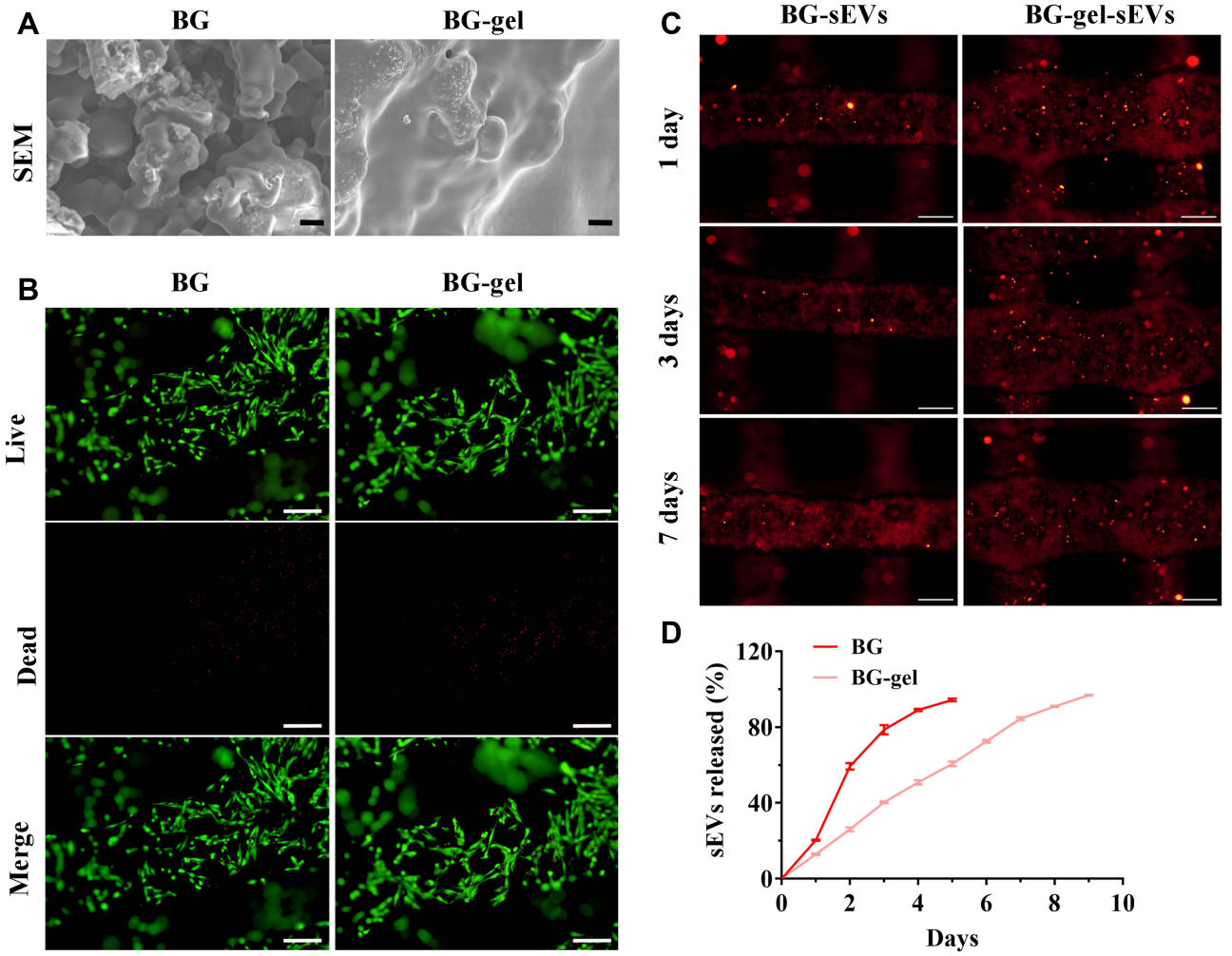

Figure 7 Characterization of engineered BG composited scaffolds. (**A**) Scanning electron micrographs of BG, BG-gel scaffolds. Scale bars: 2μm. (**B**) Fluorescence images of BMSCs stained with calcein AM (live cells stained with green fluorescence) and PI (dead cells stained with red fluorescence). Scale bars, 100μm. (**C**) Distribution of PKH-26 stained sEVs on the BG scaffold and BG-gel scaffold. Scale bars, 200μm. (**D**) Release profile of sEVs loaded by BG-gel scaffold.

showed a slow-release profile from the BG-gel-sEVs scaffolds. As seen from Supplementary Figure 4, the OD values were enhanced during the process of culture, indicating that the materials have favorable biocompatibility and without cytotoxicity. Moreover, sEVs were slow-released when encapsulated into the BG-gel samples (Figure 7D). As shown in Supplementary Figure 5, sEVs exhibited a spherical microvesicle structure under TEM, and pkh-26 labeled sEVs were endocytosed by the cells, indicating that sEVs released from scaffold were still intact and functional.

Effect of BG-Gel-sEVs Scaffold on Bone Regeneration in vivo

To construct biomimetic structural environment and ensure in vivo sustained efficacy of sEVs for efficient and high-quality bone regeneration, we fabricated 3D-printed bioglass (BG) scaffold with Gelma/nanoclay hydrogel coatings to load sEVs (BG-gel-sEVs) to achieve cell-free bone regeneration.

To address in vivo the potential of BG-gel-sEVs treatment for bone defect, the mice critical calvarial bone defects were established. After 12 weeks of operation, micro-CT was utilized to assess the calvarial bone repair. The re-constructional micro-CT images showed that the defect regions were barely covered by the regenerated bone tissue on BG group, while more newly formed bone tissue was observed in the defect regions on BG-gel-sEVs groups, compared to BG group and BG-gel groups (Figure 8A). Moreover, the results of bone volume to tissue volume ratio (BV/TV) revealed that the value on BG-gel-sEVs group was significantly higher than other two groups (Figure 8B). Bone mineral density (BMD), an important index reflecting the quality of the newly formed bone tissue, revealed the same phenomenon with BV/TV (Figure 8C). Additionally, the double fluorescence labeling including calcein and alizarin red was used to further assess bone regeneration. Green calcein labeling and Alizarin red reflected dynamic bone regeneration of 5–8 weeks and 9–12 weeks post-surgery respectively (Figure 8D). As shown in (Figure 8E and F), larger fluorochrome areas of green calcein labeling and Alizarin red labeling were observed on BG-gel-sEVs group than other two groups.

Adequate vascular network is essential for the efficient and high-quality bone regeneration. To further evaluate angiogenic effect of BG-gel-sEVs in vivo, microfill was used to reconstruct intracranial vascular after 12 weeks of operation. The regenerated blood vessels in detective regions were shown in (Figure 9A and B). The result revealed that the vascular network regenerated on BG-gel-sEVs group was significantly denser than that on other two groups. BG-gel-sEVs group exhibited the greatest extent of vascularization (Figure 9C). Furthermore, as a specific marker of vein endothelial cells, CD31 was selected to label the newly formed blood vessels in detective region. As shown in Figure 9D–F), the number and area of CD31 positive vascular on BG-gel-sEVs group was significantly increased compared to BG and BG-gel groups, indicating that hUC-MSCs-sEVs contributed to the regeneration of blood vessels in vivo.

Histological Evaluation of Calvarial Bone Defects Repaired by BG-Gel-sEVs Scaffolds

Histological staining was performed to further evaluate the efficacy of hUC-MSCs-sEVs on calvarial bone defects. A mass of fibrous connective tissue which was blue staining by Masson's trichrome staining was filled in the defect area, and few of regenerated bone tissue was presented in BG group. In contrast, the defect region in BG-gel-sEVs group was filled with some newly formed bone tissue with more integrity and maturity which was red staining by Masson's trichrome staining and only a small quality of fibrous connective tissue was observed (Figure 10A and B). Moreover, the undecalcificated bones slicing was stained in the Van Gieson picro-fuchsin staining (Figure 10C), and the results showed that more new bone stained in red staining were formed in the BG-gel-sEVs group than those in the BG and BG-gel group. The immunohistochemical staining was performed to assess the expression of osteocalcin (OCN) in the regenerated bone tissues (Figure 10D). Similar to the results of HE and Masson's trichrome staining, the expression level of OCN in BG-gel-sEVs group was enhanced compared to the BG and BG-gel group, indicating that hUC-MSCs-sEVs contributed to the bone regeneration.

Discussion

Osteogenesis and angiogenesis are critical factors for the efficient and high-quality bone regeneration.[42] Adequate vascular network is able to support the growth and proliferation of the osteoblast by delivering nutrients, oxygen and removing metabolic waste.[43,44] Thus, adequate vascular network is essential for achieving vascularized bone

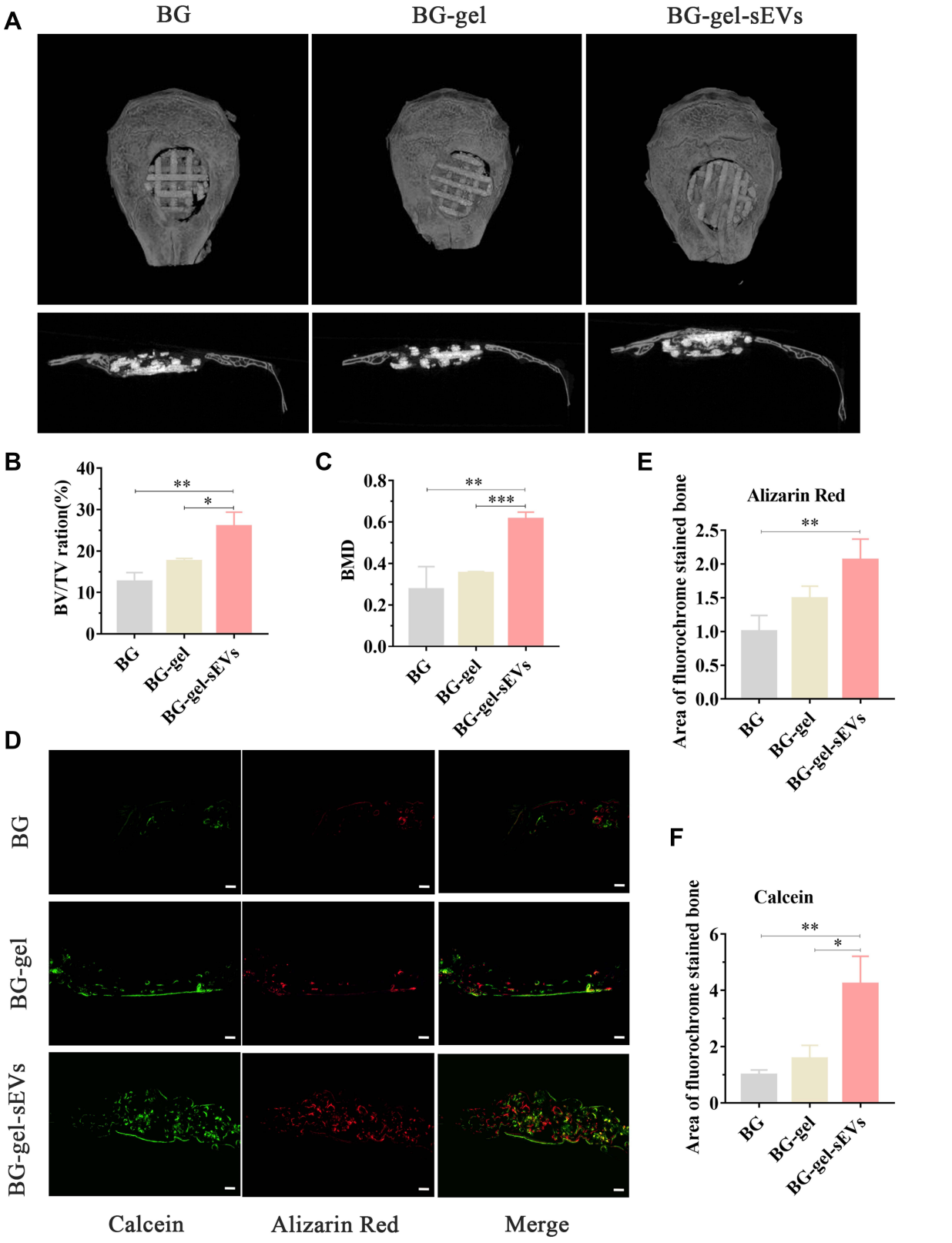

Figure 8 Micro-CT and morphometric assessment of calvarial defect repaired by BG-gel-sEVs scaffold. (**A**) Representative coronal and sagittal micrograph of bone defect. (**B** and **C**) Quantitative analysis of the new bone including bone volume/tissue volume (BV/TV), bone mineral density (BMD). Three independent replicates have been statistical analysis. *P < 0.05, **P < 0.01, ***P < 0.001. (**D**) Sequential fluorescent labeling of the regenerated bone by calcein and alizarin red. Scale bar: 200um. (**E** and **F**) Quantitative analysis of each dye area for different scaffolds, and the results of BG group was classified as one. Three independent replicates have been statistical analysis. *P < 0.05, **P < 0.01.

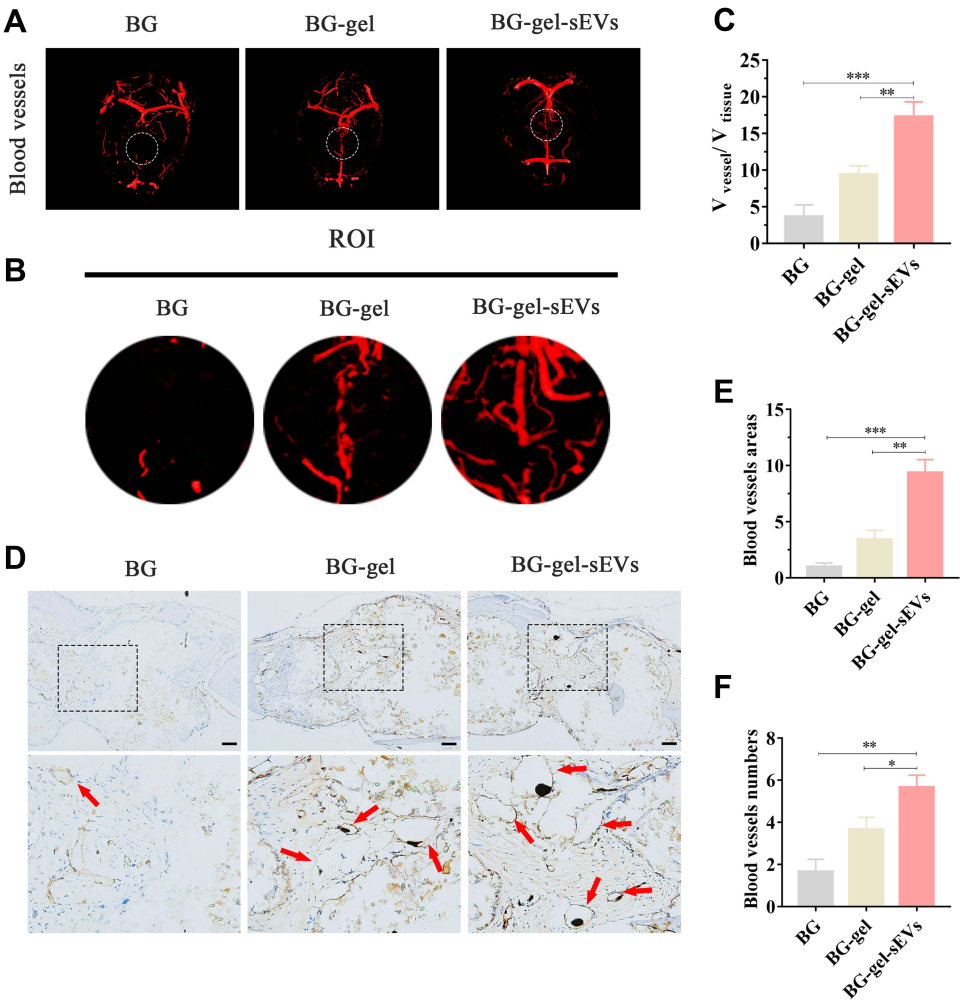

Figure 9 Effect of BG-gel-sEVs scaffold on vascularization in vivo. (**A**) Regenerated blood vessels (within the white circle) scanned by Micro-CT in the defect regions repaired by different scaffolds. (**B**) Regenerated blood vessels in regions of interest (ROI) selected for measuring the blood vessel volume. (**C**) Quantitative analysis for regenerated blood vessels. Three independent replicates have been statistical analysis. **P < 0.01, ***P < 0.001. (**D**) CD31 immunohistochemical staining was used to observe the newly formed blood vessels in the defect regions. The quantitative analysis of blood vessels area (**E**) and number (**F**). Three independent replicates have been statistical analysis. *P < 0.05, **P < 0.01, ***P < 0.001.

regeneration. Currently, various therapies for critical size bone defect have been reported.[4–6] However, the application of these therapies was limited due to their own drawbacks.[4] Herein, we extracted sEVs from hUC-MSCs, and then sEVs were co-incubated with BMSCs, the results revealed that hUC-MSCs-sEVs remarkably improved the proliferation, migration and osteogenic differentiation of BMSCs by transporting miR-23a-3p. Moreover, hUC-MSCs-sEVs could improve angiogenesis in vitro by enhancing the tube formation ability of HUVECs. Furthermore, we constructed ideal bone-grafting BG-gel scaffold with the favorable mechanical property to loading therapeutic sEVs to achieve their slow release.

hUC-MSCs are ideal cell source for MSCs-based therapy due to the favorable properties including rich sources, desirable proliferation capability and facilitated acquisition process.[14] sEVs possess specific advantages than MSCs including high stability, facilitated acquisition and abundant sources.[25] Wu et al investigated the therapeutic efficacy of MSC-derived sEVs on OA treatment, and found that sEVs promoted the chondrogenesis of BMSCs.[13] Notably, stem cells might determine the biological functions of the derived sEVs in turn.[45] Recent studies reported that MSCs-sEVs promoted angiogenesis and osteogenesis to achieve vascularized bone regeneration.[46,47] Nevertheless, the effect of hUC-MSCs-sEVs on vascularized bone regeneration is still unknown and the potential mechanism remains to be investigated.

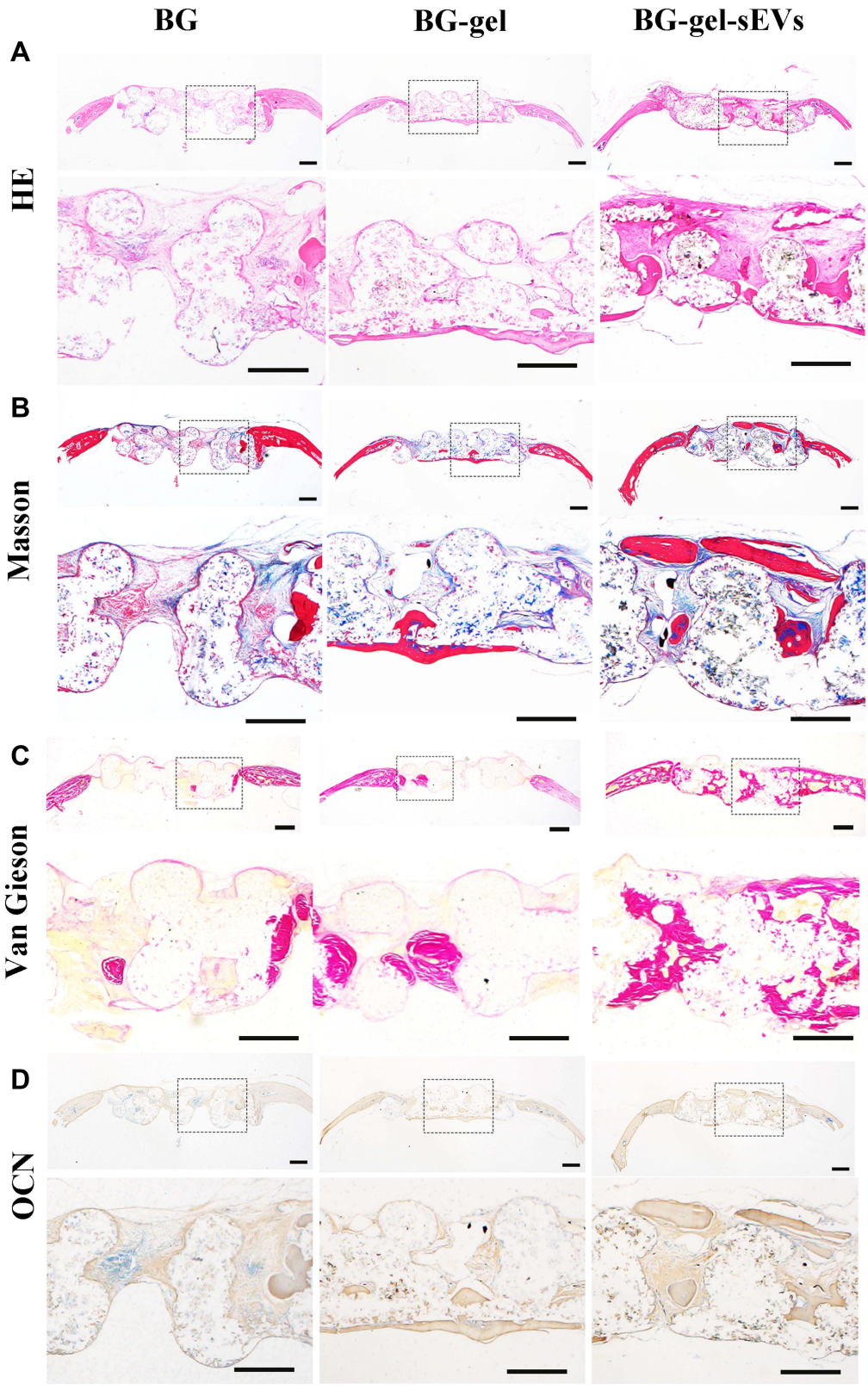

Figure 10 Histological evaluation of calvarial bone defects repaired by BG-gel-sEVs scaffolds. (**A**) HE staining and (**B**) Masson's trichrome staining of decalcified bone samples repaired by different scaffolds. Scale bar: 500um. (**C**) Van Gieson's staining of regenerated bone repaired by different scaffolds. Scale bar: 500um. (**D**) Immunohistochemical staining of OCN. Scale bar: 500um.

Herein, our study showed that hUC-MSCs-sEVs could be uptaken by BMSCs and then facilitated the proliferation, migration of BMSCs, indicating that BMSCs migrated to the defect area and further proliferated which induced by hUC-MSCs-sEVs. Additionally, hUC-MSCs-sEVs promoted the osteogenic differentiation of BMSCs, resulting in alkaline phosphatase (ALP) activation and calcium deposition. ALP activity is considered to the indicator the presence of osteoblast cells and the formation of new bone. The release of calcium ions regulated the activation of osteoblast which was conducive to bone regeneration.[48] The above results demonstrated that hUC-MSCs-sEVs were conducive to osteogenesis in vitro. Notably, bone repair and remodeling are the complicated process which involves angiogenic and osteogenic interaction.[49] For large segmental bone regeneration, favorable nutrient exchange and adequate oxygen supply transported by vascular network are beneficial for cell migration and distribution, making newly formed bone tissue grow margin-to-center.[42] Hu et al demonstrated that BMSCs-derived exosomes promoted the function and angiogenesis ability of HUVECs,[20] suggesting that MSC-derived exosomes have great potential on angiogenesis. To further evaluate the function of hUC-MSCs-sEVs on angiogenesis in vitro, HUVECs were co-incubated with hUC-MSCs-sEVs. The results revealed that hUC-MSCs-sEVs could enhance the proliferation, migration and tube formation ability of HUVECs, indicating that hUC-MSCs-sEVs could regulate the function and activity of HUVECs, improving angiogenesis in vitro. Consistently, hUC-MSCs-sEVs possess great therapeutic potential in critical size bone defect due to the ability of coupling osteogenesis and angiogenesis.

As the carriers produced by derived cells, sEVs delivered bioactive ingredient including nucleic acids, proteins, lipids and other signaling molecules to recipient cells, facilitating intercellular communication.[50] MiRNA, a class of small noncoding RNA, plays critical regulatory role in gene expression by directly modifying mRNA at post-transcriptional level.[51,52] Recent studies have reported that exosomal miRNAs played essential regulatory role in bone and vascular homoeostasis.[53,54] In previous study, we demonstrated that miR-23a-3p was highly expressed in hUC-MSCs-sEVs.[25] Meanwhile, the role of exosomal miR-23a-3p in osteogenesis and angiogenesis remains elusive. Thus, to further investigate the role of exosomal miR-23a-3p in BMSCs and HUVECs, we co-cultured sEVs with cells and found that the expression of miR-23a-3p in BMSCs and HUVECs was increased. Moreover, luciferase assay showed that miR-23a-3p mimic down-regulated the expression of PTEN, whereas miR-23a-3p mutant promoted the production of PTEN, indicating that miR-23a-3p bound the 3'UTR of PTEN, resulting in the down regulation of PTEN. Previous study showed that PTEN played negative regulated role in AKT signaling pathway.[55] The activation of PTEN/AKT signaling pathway promoted BMSCs osteogenic differentiation.[41] In this study, we demonstrated that hUC-MSCs-sEVs promoted angiogenesis and osteogenesis in vitro by delivering miR-23a-3p. The up-regulated miR-23a-3p in cells targeted mRNA of PTEN and suppressed the expression of PTEN, resulting in the activation of AKT signaling pathway. Additionally, the downregulated miR-23a-3p in cells induced by antogomirs-23a weaken the effect of angiogenesis and osteogenesis which induced by hUC-MSCs-sEVs. In general, hUC-MSCs-sEVs may be a promising therapeutic treatment for critical size bone defect.

Subsequently, we fabricated BG scaffold with Gelma/nanoclay hydrogel coatings to load sEVs to achieve continuously therapeutic effect in vivo. Bioglass scaffolds with excellent mechanical, osteo-inductive and controlled degradation property are the ideal biomaterial in cell-free bone tissue engineering.[1,4,32] Previous study revealed that hUC-MSCs-sEVs entrapped into Gelma/nanoclay hydrogels were released in a sustained manner through the controlled degradation of hydrogel.[25] Herein, we fabricated BG-gel-sEVs composited scaffolds to achieve vascularized bone regeneration. In vivo results showed that BG-gel-sEVs composited scaffold effectively improved angiogenesis and osteogenesis, repairing skull bone defect.

Conclusions

In general, our study found that hUC-MSCs-sEVs effectively improved angiogenesis and osteogenesis by delivering miR-23a-3p to activate PTEN/AKT signaling pathway in vitro. Additionally, the BG-gel-sEVs composited scaffold achieved vascularized bone regeneration by slowly releasing sEVs. Consistently, the BG-gel-sEVs composited scaffold has essential potential in skull bone defect treatment.

Acknowledgments

We would like to thank Xinlu Liu for Scheme drawing of the manuscript. We are grateful to Mr. Shuxiang Fu and Mr. Liang Yu (Promab Biotechnologies) for their support and assistance.

Author Contributions

All authors made a significant contribution to the work reported, whether that is in the conception, study design, execution, acquisition of data, analysis and interpretation. All authors gave final approval of the version to be published and have agreed on the journal to which the article has been submitted.

Funding

This work was supported by the National Natural Science Foundation of China (81802202, 51673212, 82172437), the Natural Science Foundation of Shanghai (19ZR1455900), the International Cooperation Project of National Natural Science Foundation of China (81810001048) and Shanghai Key Clinical Specialty Construction Project - Spinal Surgery (WSJ1916, WSJ1714).

Disclosure

The authors declare no potential conflicts of interest in this work.

References

1. Chen R, Wang J, Liu CS. Biomaterials act as enhancers of growth factors in bone regeneration. *Adv Funct Mater*. 2016;26(48):8810–8823.
2. Mao G, Zhang Z, Hu S, et al. Exosomes derived from miR-92a-3p-overexpressing human mesenchymal stem cells enhance chondrogenesis and suppress cartilage degradation via targeting WNT5A. *Stem Cell Res Ther*. 2018;9(1):247.
3. Aldemir Dikici B, Reilly GC, Claeyssens F. Boosting the osteogenic and angiogenic performance of multiscale porous polycaprolactone scaffolds by in vitro generated extracellular matrix decoration. *ACS Appl Mater Interfaces*. 2020;12(11):12510–12524.
4. Garot C, Bettega G, Picart C. Additive manufacturing of material scaffolds for bone regeneration: toward application in the clinics. *Adv Funct Mater*. 2021;31(5):2006967.
5. Huang JH, Yin XM, Xu Y, et al. Systemic administration of exosomes released from mesenchymal stromal cells attenuates apoptosis, inflammation, and promotes angiogenesis after spinal cord injury in rats. *J Neurotrauma*. 2017;34(24):3388–3396.
6. Chocholata P, Kulda V, Babuska V. Fabrication of scaffolds for bone-tissue regeneration. *Materials*. 2019;12(4):568.
7. Du Z, Feng X, Cao G, et al. The effect of carbon nanotubes on osteogenic functions of adipose-derived mesenchymal stem cells in vitro and bone formation in vivo compared with that of nano-hydroxyapatite and the possible mechanism. *Bioactive Materials*. 2021;6(2):333–345.
8. Dominici M, Le Blanc K, Mueller I, et al. Minimal criteria for defining multipotent mesenchymal stromal cells. The International Society for Cellular Therapy position statement. *Cytotherapy*. 2006;8(4):315–317.
9. Liu X, Rui T, Zhang S, Ding Z. Heterogeneity of MSC: origin, molecular identities, and functionality. *Stem Cells Int*. 2019;2019:9281520.
10. Squillaro T, Peluso G, Galderisi U. Clinical trials with mesenchymal stem cells: an update. *Cell Transplant*. 2016;25(5):829–848.
11. Galderisi U, Peluso G, Di Bernardo G. Clinical trials based on mesenchymal stromal cells are exponentially increasing: where are we in recent years? *Stem Cell Rev Rep*. 2022;18(1):23–36.
12. Phinney DG. Functional heterogeneity of mesenchymal stem cells: implications for cell therapy. *J Cell Biochem*. 2012;113(9):2806–2812.
13. Wu J, Kuang L, Chen C, et al. miR-100-5p-abundant exosomes derived from infrapatellar fat pad MSCs protect articular cartilage and ameliorate gait abnormalities via inhibition of mTOR in osteoarthritis. *Biomaterials*. 2019;206:87–100.
14. Yang W, Zhang J, Xu B, et al. HucMSC-derived exosomes mitigate the age-related retardation of fertility in female mice. *Mol Ther*. 2020;28(4):1200–1213.
15. Wang M, Wang C, Chen M, et al. Efficient angiogenesis-based diabetic wound healing/skin reconstruction through bioactive antibacterial adhesive ultraviolet shielding nanodressing with exosome release. *ACS nano*. 2019;13:10279.
16. Zhang ZG, Buller B, Chopp M. Exosomes - beyond stem cells for restorative therapy in stroke and neurological injury. *Nat Rev Neurol*. 2019;15(4):193–203.
17. Swanson WB, Zhang Z, Xiu KM, et al. Scaffolds with controlled release of pro-mineralization exosomes to promote craniofacial bone healing without cell transplantation. *Acta Biomaterialia*. 2020;118:215–232.
18. Kalluri R, LeBleu VS. The biology, function, and biomedical applications of exosomes. *Science*. 2020;367(6478):eaau6977.
19. Fitts CA, Ji N, Li Y, Tan C. Exploiting exosomes in cancer liquid biopsies and drug delivery. *Adv Healthc Mater*. 2019;8(6):e1801268.
20. Hu YQ, Tao RY, Chen L, et al. Exosomes derived from pioglitazone-pretreated MSCs accelerate diabetic wound healing through enhancing angiogenesis. *J Nanobiotechnol*. 2021;19(1):1–7.
21. Li CJ, Cheng P, Liang MK, et al. MicroRNA-188 regulates age-related switch between osteoblast and adipocyte differentiation. *J Clin Invest*. 2015;125(4):1509–1522.
22. Mayya VK, Flamand MN, Lambert AM, et al. microRNA-mediated translation repression through GYF-1 and IFE-4 in C. elegans development. *Nucleic Acids Res*. 2021;49(9):4803–4815.
23. Thind A, Wilson C. Exosomal miRNAs as cancer biomarkers and therapeutic targets. *J Extracell Vesicles*. 2016;5:31292.
24. Gao ZS, Zhang CJ, Xia N, et al. Berberine-loaded M2 macrophage-derived exosomes for spinal cord injury therapy. *Acta Biomater*. 2021;126:211–223.
25. Hu H, Dong L, Bu Z, et al. miR-23a-3p-abundant small extracellular vesicles released from Gelma/nanoclay hydrogel for cartilage regeneration. *J Extracell Vesicles*. 2020;9(1):1778883.
26. Chen P, Zheng L, Wang Y, et al. Desktop-stereolithography 3D printing of a radially oriented extracellular matrix/mesenchymal stem cell exosome bioink for osteochondral defect regeneration. *Theranostics*. 2019;9(9):2439–2459.
27. Tao SC, Guo SC, Li M, Ke QF, Guo YP, Zhang CQ. Chitosan wound dressings incorporating exosomes derived from MicroRNA-126-overexpressing synovium mesenchymal stem cells provide sustained release of exosomes and heal full-thickness skin defects in a diabetic rat model. *Stem Cells Transl Med*. 2017;6(3):736–747.

28. Wang M, Wang CG, Chen M, et al. Efficient angiogenesis-based diabetic wound healing/skin reconstruction through bioactive antibacterial adhesive ultraviolet shielding nanodressing with exosome release. *Acs Nano*. 2019;13(9):10279–10293.
29. Chen S, Tang Y, Liu Y, et al. Exosomes derived from miR-375-overexpressing human adipose mesenchymal stem cells promote bone regeneration. *Cell Prolif*. 2019;52(5):e12669.
30. Xu B, Zheng PB, Gao F, et al. Strength and tough hydrogel for skull bone regeneration. *Adv Funct Mater*. 2017;27(4):1604327.
31. Nonoyama T, Wada S, Kiyama R, et al. Double-network hydrogels strongly bondable to bones by spontaneous osteogenesis penetration. *Adv Mater*. 2016;28(31):6740–6745.
32. Zhai MM, Zhu Y, Yang MY, Mao CB. Human mesenchymal stem cell derived exosomes enhance cell-free bone regeneration by altering their miRNAs profiles. *Adv Sci*. 2020;7(19):2001334.
33. Wang C, Hu H, Li Z, et al. Enhanced osseointegration of titanium alloy implants with laser microgrooved surfaces and graphene oxide coating. *ACS Appl Mater Interfaces*. 2019;11(43):39470–39483.
34. Lin C, Liu L, Zeng C, et al. Activation of mTORC1 in subchondral bone preosteoblasts promotes osteoarthritis by stimulating bone sclerosis and secretion of CXCL12. *Bone Res*. 2019;7:5.
35. Liu L, Liu Y, Feng C, et al. Lithium-containing biomaterials stimulate bone marrow stromal cell-derived exosomal miR-130a secretion to promote angiogenesis. *Biomaterials*. 2019;192:523–536.
36. Zhu Z, Liu Y, Xue Y, et al. Tazarotene released from aligned electrospun membrane facilitates cutaneous wound healing by promoting angiogenesis. *ACS Appl Mater Interfaces*. 2019;11(39):36141–36153.
37. Baino F, Magnaterra G, Fiume E, et al. Digital light processing stereolithography of hydroxyapatite scaffolds with bone-like architecture, permeability, and mechanical properties. *J Am Ceram Soc*. 2021;105:1648.
38. Wei L, Wu S, Kuss M, et al. 3D printing of silk fibroin-based hybrid scaffold treated with platelet rich plasma for bone tissue engineering. *Bioact Mater*. 2019;4:256–260.
39. Chen Y, Wu T, Huang S, et al. Sustained release SDF-1alpha/TGF-beta1-loaded silk fibroin-porous gelatin scaffold promotes cartilage repair. *ACS Appl Mater Interfaces*. 2019;11(16):14608–14618.
40. DiStefano TJ, Vaso K, Danias G, Chionuma HN, Weiser JR, Iatridis JC. Extracellular vesicles as an emerging treatment option for intervertebral disc degeneration: therapeutic potential, translational pathways, and regulatory considerations. *Adv Healthcare Mater*. 2021;11:2100596.
41. Jin CY, Jia LF, Tang ZH, Zheng YF. Long non-coding RNA MIR22HG promotes osteogenic differentiation of bone marrow mesenchymal stem cells via PTEN/AKT pathway. *Cell Death Dis*. 2020;11(7):1–3.
42. Han X, Sun M, Chen B, et al. Lotus seedpod-inspired internal vascularized 3D printed scaffold for bone tissue repair. *Bioact Mater*. 2021;6(6):1639–1652.
43. Frohlich LF. MicroRNAs at the interface between osteogenesis and angiogenesis as targets for bone regeneration. *Cells-Basel*. 2019;8(2):121.
44. Chen MJ, Zhang YH, Zhang WA, Li J. Polyhedral oligomeric silsesquioxane-incorporated gelatin hydrogel promotes angiogenesis during vascularized bone regeneration. *Acs Appl Mater Inter*. 2020;12(20):22410–22425.
45. Jing H, Zhang X, Luo K, et al. miR-381-abundant small extracellular vesicles derived from kartogenin-preconditioned mesenchymal stem cells promote chondrogenesis of MSCs by targeting TAOK1. *Biomaterials*. 2020;231:119682.
46. Liu L, Yu F, Li L, et al. Bone marrow stromal cells stimulated by strontium-substituted calcium silicate ceramics: release of exosomal miR-146a regulates osteogenesis and angiogenesis. *Acta Biomater*. 2021;119:444–457.
47. Zha Y, Li YW, Lin TY, Chen J, Zhang SM, Wang JL. Progenitor cell-derived exosomes endowed with VEGF plasmids enhance osteogenic induction and vascular remodeling in large segmental bone defects. *Theranostics*. 2021;11(1):397–409.
48. Jeong J, Kim JH, Shim JH, Hwang NS, Heo CY. Bioactive calcium phosphate materials and applications in bone regeneration. *Biomater Res*. 2019;23(1):1.
49. Wang XT, Li XL, Li J, et al. Mechanical loading stimulates bone angiogenesis through enhancing type H vessel formation and downregulating exosomal miR-214-3p from bone marrow-derived mesenchymal stem cells. *FASEB J*. 2021;35(1):e21150.
50. Nakao Y, Fukuda T, Zhang Q, et al. Exosomes from TNF-alpha-treated human gingiva-derived MSCs enhance M2 macrophage polarization and inhibit periodontal bone loss. *Acta Biomater*. 2021;122:306–324.
51. Li Y, Fan C, Wang L, et al. MicroRNA-26a-3p rescues depression-like behaviors in male rats via preventing hippocampal neuronal anomalies. *J Clin Invest*. 2021;131. doi:10.1172/JCI148853
52. Ito Y, Matsuzaki T, Ayabe F, et al. Both microRNA-455-5p and −3p repress hypoxia-inducible factor-2alpha expression and coordinately regulate cartilage homeostasis. *Nat Commun*. 2021;12(1):4148.
53. Liu A, Lin D, Zhao H, et al. Optimized BMSC-derived osteoinductive exosomes immobilized in hierarchical scaffold via lyophilization for bone repair through Bmpr2/Acvr2b competitive receptor-activated Smad pathway. *Biomaterials*. 2021;272:120718.
54. Aday S, Hazan-Halevy I, Chamorro-Jorganes A, et al. Bioinspired artificial exosomes based on lipid nanoparticles carrying let-7b-5p promote angiogenesis in vitro and in vivo. *Mol Ther*. 2021;29(7):2239–2252.
55. Manning BD, Toker A. AKT/PKB Signaling: navigating the network. *Cell*. 2017;169(3):381–405.